Letter

Thermodynamic properties of mixed-valent Eu ions and nonmetallicity in $Eu_3Bi_2S_4F_4$ single crystals

Ryuji Higashinaka,* Hideaki Endo, Joe Kajitani, Ryotaro Sakatani, Tatsuma D. Matsuda, and Yuji Aoki†
Department of Physics, Tokyo Metropolitan University, Hachioji, Tokyo 192-0397, Japan

(Received 22 February 2023; accepted 6 July 2023; published 25 August 2023)

New BiS_2-based layered compound $Eu_3Bi_2S_4F_4$ has recently been reported to exhibit superconductivity with a transition temperature of 1.5 K using polycrystalline samples. Here we report measurements of electrical resistivity ρ, magnetization M, and specific heat C of $Eu_3Bi_2S_4F_4$ single crystals. At the antiferromagnetic transition temperature of 2.17 K, $C(T)$ shows a sharp λ-type peak, suggesting the existence of strong Eu magnetic moment fluctuations due to the quasi-two-dimensional nature of the Eu-ion lattice in Eu_3F_4 block layers. The average Eu-ion valence of +2.19, determined from the Schottky-type $4f$-electron contribution to $C(T)$ and $M(T,H)$, indicates the self-doped electron density in BiS_2 layers due to the Eu mixed valence to be 0.285 electrons per Bi site. It has been revealed, however, that $\rho(T)$ shows an anomalous nonmetallic behavior with $\sim 1/T^3$ dependence without any sign of superconductivity, in marked contrast to a metallic behavior in the polycrystals. This behavior suggests an unconventional electron-localization mechanism working in the single crystals, possibly caused by Eu^{2+}/Eu^{3+} distribution (or fluctuations) and/or lattice instabilities inherent to BiS_2 layers.

DOI: 10.1103/PhysRevB.108.L081122

The recent discovery of superconductivity (SC) in BiS_2-based layered materials [1–4] has attracted considerable attention because of the crystal similarity with cuprates [5] and Fe-based superconductors [6]. The typical parent material $REOBiS_2$ (RE: Rare-earth elements) is usually a band insulator. The band filling can be controlled by electron doping through partial substitution of F for O [2] or of tetravalent ions for trivalent RE ions [7,8]. As the doping level increases, the system becomes more metallic and SC develops within BiS_2 layers. The conduction bands are composed of Bi $6p_{x/y}$ orbitals giving rise to rectangular electron pockets around the X points of the Brillouin zone [9–11], providing the two-dimensional (2D) nature of the transport properties [12,13]. On the other hand, $4f$ electrons of rare-earth ions located in block layers exhibit a wide variety of interesting phenomena, including a quantum critical behavior of Ce magnetic moments in $CeOFBiS_2$ possibly caused by geometrical frustration [14], emergent SC of self-doped carriers in BiS_2 layers caused by mixed-valent Ce and Eu ions [15–21], and SC coexisting with ferromagnetic ordering in $CeO_{1-x}F_xBiS_2$ [22–24] and with antiferromagnetic ordering in $EuOBiS_2$ [18,19].

$Eu_3Bi_2S_4F_4$ is a new family member of the BiS_2-based compounds [25]. It crystallizes in a tetragonal structure with the space group $I4/mmm$ (#139) (see Fig. 1). A CaF_2-type Eu_3F_4-layer and a BiS_2-bilayer stack alternately along the [001] direction. Eu ions occupy two inequivalent crystallographical sites: Eu(1) [$4e$ ($4mm$)] and Eu(2) [$2a$ ($4/mmm$)]. One of the most interesting features of $Eu_3Bi_2S_4F_4$ is the intermediate Eu valence between Eu^{2+} and Eu^{3+}. In polycrystals, the average valence of Eu ions (v_{Eu}) was estimated to be +2.2 by the bond-valence-sum analysis, ^{151}Eu Mössbauer spectroscopy and magnetic susceptibility [25]. This feature should lead to self-electron-doping into BiS_2 layers. The polycrystalline sample, indeed, shows a metallic behavior and SC sets in at $T_c = 1.5$ K [25] without any substitution. At 2.3 K($> T_c$), there sets in an antiferromagnetic (AFM) ordering, which coexists with the SC state below T_c. Most of the studies on $Eu_3Bi_2S_4F_4$ including hydrostatic pressure effect [26,27] and substitution effects [28–31] have been made so far using polycrystalline samples. Studies of the BiS_2-based materials using single crystals have revealed that the strongly anisotropic behaviors of electrical transport [32,33], superconductivity [34,35], and magnetism of rare-earth ions in block layers [14]. Therefore, it is highly desired to investigate $Eu_3Bi_2S_4F_4$ single crystals to clarify further the intrinsic physical properties of this material. Recently, we have succeeded in growing single crystals by CsCl-flux method [36]. In this Letter, we report measurements of the electrical resistivity, magnetization, and specific heat of $Eu_3Bi_2S_4F_4$ single crystals. Single crystals of $Eu_3Bi_2S_4F_4$ have been grown by CsCl-flux method using starting materials consisting of 3N (99.9% pure)-EuS, 5N-Bi_2S_3, 4N-BiF_3, 3N-S, and 3N-CsCl (see Refs. [36] and [37] for details). Using these single crystals, Eu L_3-edge x-ray absorption spectroscopy (XAS) and space-resolved angle-resolved photoemission spectroscopy (ARPES) have been measured [40]. The former provides the average Eu-ion valence $v_{Eu} = 2.20(2)$. The latter clarified the formation of an electron-like pocket centered at each of the X points (anomalous missing intensity around E_F will be

*higashin@tmu.ac.jp
†aoki@tmu.ac.jp

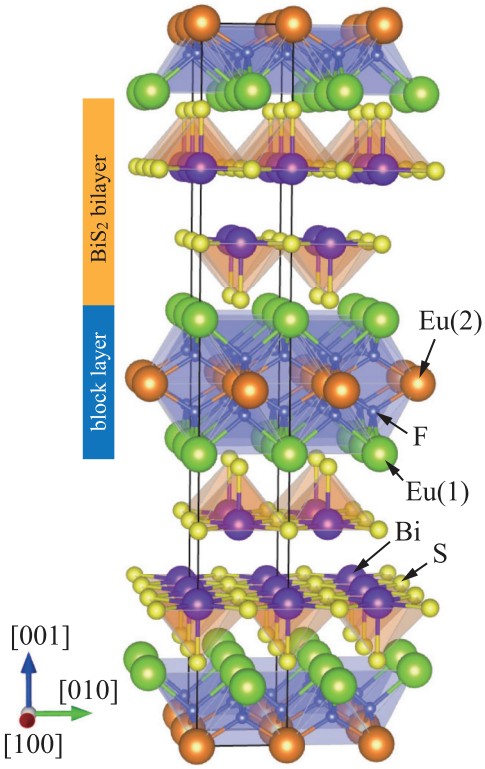

FIG. 1. Crystal structure of $Eu_3Bi_2S_4F_4$ ($I4/mmm$, #139, $Z = 2$), which has two crystallographically distinct Eu sites, Eu(1) [4e (4mm)] and Eu(2) [2a (4/mmm)]. The unit cell is depicted by thin lines.

discussed below), and the Luttinger volume analysis provides the doped electron density to be $n = 0.23$ electrons per Bi site, which corresponds to $v_{\mathrm{Eu}} = 2 + 2n/3 = 2.15$. In addition, it has confirmed that v_{Eu} is uniform in the crystals, ruling out the possibility of any microscale phase separation.

The electrical resistivity ρ was measured by a standard four-probe technique using a Quantum Design (QD) Physical Property Measurement System (PPMS) equipped with a ^{3}He option down to 0.6 K. The dc magnetization M was measured using a QD Magnetic Property Measurement System down to 2 K in applied fields up to 7 T. The ac magnetic susceptibility χ_{ac} was measured by a mutual inductance method down to 0.18 K with a modulation field of $H_{\mathrm{ac}} = 0.3$ Oe using a ^{3}He - ^{4}He dilution refrigerator. The specific heat was measured by a quasiadiabatic heat pulse method using the PPMS and the dilution refrigerator down to 0.14 K and in applied fields up to 9 T. All the measurements in $H \neq 0$ were performed with increasing temperature after field cooling down to the lowest temperature. The temperature dependence of electrical resistivity $\rho(T)$ of a $Eu_3Bi_2S_4F_4$ single crystal is shown in Fig. 2. The data show an extremely strong nonmetallic behavior ($d\rho/dT < 0$) over the measured temperature range down to 0.7 K; $\rho(0.7\ \mathrm{K})/\rho(300\ \mathrm{K})$ reaches about $\sim 10^7$. $\rho(T)$ shows an anomalous power-law T dependence expressed as αT^n with $\alpha = 234.6(1)\ \Omega\mathrm{m/K}^n$ and $n = -2.99$ over the wide temperature range of about an order of magnitude below 30 K. In the AFM state, ρ deviates upward slightly from the extrapolated αT^n curve [see Fig. 2(a) for an expanded view]. Above $\sim$70 K, as shown in a $\ln(\rho)$ vs $1/T$

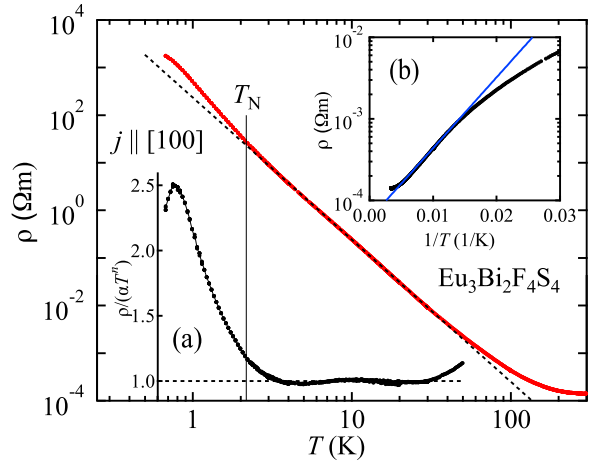

FIG. 2. Temperature dependence of electrical resistivity ρ of a $Eu_3Bi_2S_4F_4$ single crystal for the current flow along the [100] direction. Anomalous power-law T dependence expressed as αT^n [$\alpha = 234.6(1)\ \Omega\mathrm{m/K}^n$ and $n = -2.99$] is shown by dotted line. Inset (a): $\rho/(\alpha T^n)$ vs $\log T$. Inset (b): $\log(\rho)$ vs $1/T$ shows an Arrhenius-type behavior above 70 K.

plot of Fig. 2(b), $\rho(T)$ shows an Arrhenius-type behavior. A fitting to the data using $\rho = \rho_0 \exp(E_g/2T)$ provides the energy gap $E_g = 400$ K. These behaviors are in marked contrast to the reported polycrystalline data [25,26], which show a metallic behavior ($d\rho/dT > 0$) above 35 K and a weak semiconducting behavior ($d\rho/dT < 0$) below 35 K along with a SC transition in $\rho(T)$ at $T_c = 1.5$ K. This discrepancy will be discussed below. The temperature dependencies of dc magnetic susceptibility $\chi \equiv M/H$ (for $H \parallel [100]$, [110], and [001]) in 0.1 T and ac magnetic susceptibility χ_{ac} (for $H \parallel [100]$) are shown in Fig. 3. With decreasing T from RT, χ increases gradually showing a Curie-Weiss behavior. A sudden decrease appears at 2.17 K ($\equiv T_{\mathrm{N}}$), indicating the occurrence of the AFM phase transition. Below T_N, χ for $H \parallel [001]$ continues to

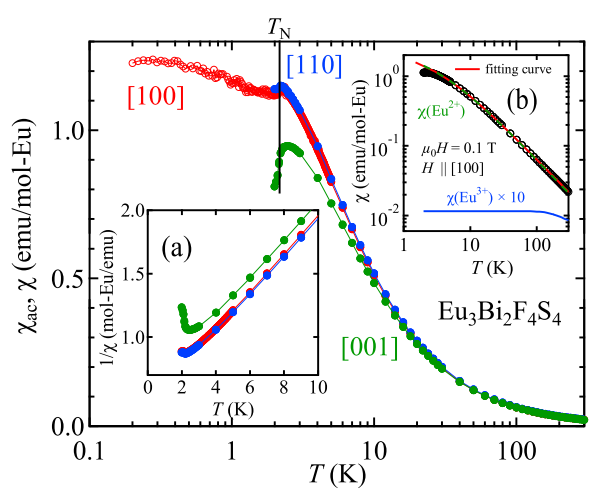

FIG. 3. Magnetic susceptibility $\chi(T)$ in $\mu_0 H = 0.1$ T along the [100], [110], and [001] directions. $\chi_{\mathrm{ac}}(T)$ measured by a mutual inductance method with a modulation field of $H_{\mathrm{ac}} = 0.3$ Oe ($\mu_0 H_{\mathrm{ac}} \parallel [100]$) is also shown. Inset (a): $1/\chi$ vs T below 10 K. Inset (b): $\chi(T)$ consists of Eu^{2+} and Eu^{3+} contributions.

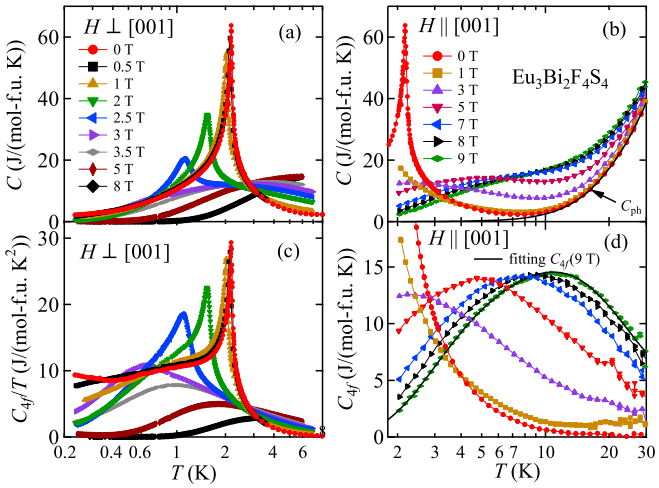

FIG. 4. Specific heat $C(T)$ for (a) $H \perp [001]$ ($0.2 < T < 8$ K) and (b) $H \parallel [001]$ ($1.8 < T < 30$ K). [(c) and (d)] The $4f$ electron contribution $C_{4f}(T)$ extracted from each data set.

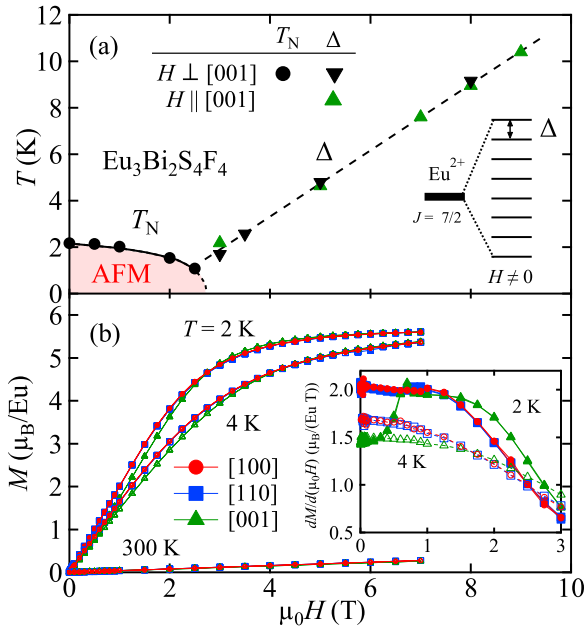

FIG. 5. (a) T-vs-H phase diagram. AFM phase boundary $T_N(H)$ for $H \perp [001]$ (closed circles) and the energy separation $\Delta(H)$ of the $J = 7/2$ multiplet of Eu^{2+} ions for $H \parallel [001]$ (solid triangles) and $H \perp [001]$ (solid inverted triangles) are shown. The schematic energy diagram representing the Zeeman splitting of the $J = 7/2$ multiplet of Eu^{2+} ions is shown in the inset. (b) Magnetization $M(H)$ and its derivative $dM/d(\mu_0 H)$ (inset) at 2 and 4 K (data taken from Ref. [36]).

decrease, while χs for $H \parallel [100]$ and $H \parallel [110]$ remain almost constant. This fact suggests that the ordered Eu magnetic moments in the AFM state are aligned along the [001] direction. Below T_N, $\chi_{ac}(T)$ is always positive and does not show any sign of Meissner signal down to 0.18 K. This result along with the $\rho(T)$ data confirms no SC transition above 0.18 K in the single crystals.

Below ~20 K, a magnetic anisotropy in χ becomes visible between $H \parallel [001]$ and $H \perp [001]$ while there is no anisotropy in the (001) plane. A $1/\chi$-vs-T plot is shown in Fig. 3(a). The effective magnetic moment of Eu ions $\mu_{eff} = 7.45(4)\ \mu_B$/Eu is almost the same for all the field directions while the paramagnetic Curie-Weiss temperature θ_p is different; $\theta_p = -4.1(-3.2)$ K for $H \parallel [001]$ ($H \perp [001]$). This fact suggests that the AFM interaction is stronger when Eu magnetic moments are parallel to the [001] direction.

The average valence of Eu ion (v_{Eu}) can be estimated from the $\chi(T)$ data, which are well reproduced using $\chi(T) = (3-v_{Eu})\chi_{Eu^{2+}} + (v_{Eu}-2)\chi_{Eu^{3+}}$, where $\chi_{Eu^{2+}} \equiv C_{Eu^{2+}}/(T-\theta_p)$ and $\chi_{Eu^{3+}}$ are the contributions from Eu^{2+} and Eu^{3+} ions. The Curie constant $C_{Eu^{2+}}$ for Eu^{2+} ions is 7.88 (emu K)/mol-Eu, which corresponds to the effective moment $\mu_{eff} = 7.94\ \mu_B$/Eu. For $\chi_{Eu^{3+}}(T)$, we employ the theoretical model for the Eu^{3+} Van Vleck paramagnetic susceptibility using the spin-orbit coupling constant $\lambda = 490$ K [37,41], which has been confirmed to reproduce $\chi(T)$ of EuF_3. A fit of the $\chi(T)$ data for $H \parallel [100]$ in $10 < T < 300$ K to the model [see Fig. 3(b)] provides $v_{Eu} = 2.19(0)$ and $\theta_p = -2.55(1)$ K. The value of v_{Eu}, in good agreement with the above-mentioned XAS and ARPES data [40], confirms that Eu ions in the $Eu_3Bi_2S_4F_4$ single crystals are certainly in a mixed valence state. The self-doped electron density in BiS_2 layers is estimated to be $n = 1.5(v_{Eu} - 2) = 0.285$ electrons per Bi site. The temperature dependence of specific heat $C(T)$ is shown in Fig. 4. In zero field, there appears a sharp λ-shaped peak at T_N. The logarithmic-like divergence of the peak reflects the quasi-2D nature of the magnetic ordering in the Eu-ion lattice, where magnetic fluctuations dominate around T_N. The peak height of 65 J/(mol-f.u. K), which is larger than that for polycrystals [25], attests to the high quality of the single crystals.

With increasing magnetic field, the peak height gradually decreases and the peak position shifts to lower temperatures, indicating the suppression of the AFM phase by magnetic fields. The AFM phase boundary determined by the peak position is depicted in a T-vs-H phase diagram of Fig. 5(a). It can be well described by $T_N(H) = T_N(0) - a(\mu_0 H)^n$ with $a = 0.126(11)$ K/T^n and $n = 2.34(10)$ for $H \perp [001]$. In $\mu_0 H > \mu_0 H_N$, there remains a broadened peak in $C(T)$, which shifts to higher temperatures with increasing $\mu_0 H$. This is a Schottky peak originating from the Zeeman splitting of $J = 7/2$ multiplet of Eu^{2+} ions.

In the measured temperature range, $C(T)$ has contributions from the $4f$ electrons (C_{4f}) and phonons (C_{ph}) [37]. From all the $C(T)$ data in $\mu_0 H \neq 0$, C_{4f} is calculated using $C_{4f} = C - C_{ph}$, where $C_{ph} = \beta T^3$ [$\beta = 2.39\times10^{-3}$ J/(mol-f.u. K^4) [37]] is assumed to be of H independence. The results are shown in Fig. 4 as (c) C_{4f}/T vs T for $H \perp [001]$ and (d) C_{4f} vs T for $H \parallel [001]$. The broad peak in the paramagnetic phase is attributable to a Schottky peak arising from the Zeeman splitting of the $J = 7/2$ multiplet of Eu^{2+} ions into eight equally spaced energy levels with a separation of $\Delta = 2\mu_B(\mu_0 H^*)/k_B$, where $\mu_0 H^*$ is the effective field acting at the Eu^{2+} sites. Therefore, C_{4f} can be expressed by $3(3 - v_{Eu})C_{Sch}^{Eu^{2+}}(\Delta, T)$, where $C_{Sch}^{Eu^{2+}}(\Delta, T)$ represents a Schottky contribution in the unit of J/(mol-Eu^{2+} K) [37]. Note that

the contributions from Eu^{3+} ions are negligible because the thermal excitation energy between the ground-state multiplet $^7F_0$ and first-excited multiplet $^7F_1$ with $\lambda = 490$ K is high enough [41]. By the fitting of the Schottky peak structures in Figs. 4(c) and 4(d), Δ is obtained and is depicted in the T-vs-H phase diagram of Fig. 5(a). These data points fall on a line, which has a slope close to that of $\Delta = 2\mu_B(\mu_0 H)/k_B = (1.343\ \mathrm{K/T}) \times \mu_0 H$ but is slightly shifted to lower temperatures, suggesting the existence of AFM interactions among Eu ions. The AFM exchange field acting on Eu^{2+} ions in the high-field paramagnetic phase is estimated as $\Delta(\mu_0 H \to 0)/(1.343\ \mathrm{K/T}) = 1.4$–$1.5$ T. In Fig. 4(d), a fitting curve for 9 T demonstrates that the present Schottky model reproduces the $C_{4f}(T)$ curve well, suggesting that $4f$ electrons of Eu ions are in a well-localized state. The best fitting parameters are $\Delta = 10.91(4)$ K and $v_{Eu} = 2.36$, which is slightly larger than 2.19 obtained from $\chi(T)$. This difference may partly be due to a possible suppression of the $C_{4f}(T)$ peak due to AFM interactions; note that similar behavior is observed in $YbPd_2Sn$ [42].

The H dependence of M is shown in Fig. 5(b). The saturation magnetization M_{sat} at 2 K is 5.6 μ_B/Eu, which is smaller than the fully polarized value for a Eu^{2+} free ion $M_{Eu^{2+}} = 7\ \mu_B$/Eu. From this difference, v_{Eu} is estimated to be $3 - M_{sat}/M_{Eu^{2+}} = +2.2$, which agrees well with $v_{Eu} = +2.19$ obtained from the $\chi(T)$ data. At 2 K, only for $H \| [001]$, $M(H)$ curve shows a concave upward curvature below 1 T, indicating the occurrence of a weak metamagnetic-like anomaly (see Supplemental Material [37]). Although the anomaly is not well developed because 2 K is close to T_N, the H dependence of $dM/d(\mu_0 H)$ at 2 K detects a sharp increase at 0.7 T as shown in the inset of Fig. 5(b). This anomaly disappears above T_N (see the data at 4 K). This feature agrees with the scenario that the AFM ordered moments are aligned along the [001] direction. No such anomalies appearing for $H \| [100]$ and $H \| [110]$ suggests that field-induced canting of Eu magnetic moments occurs easily. Note that such weak anisotropy of Eu magnetic moments in the AFM state is understandable because the orbital angular momentum of the $J = 7/2$ multiplet is $L = 0$, i.e., the $4f$ electron charge distribution has a spherical shape, indicating isotropic magnetic properties of a Eu ion in the crystalline lattice.

In comparison with the reported data for polycrystals [25], the overall behaviors of the magnetic properties of Eu ions are almost the same, i.e., $v_{Eu} = 2.19$ (2.17), $T_N = 2.17$ (2.3) K, and $M_{sat} = 5.60$ (5.59) μ_B/Eu at 2 K for the single crystals (polycrystals). This fact suggests that the electronic states of Eu_3F_4 block layers in the two samples are almost the same. Nevertheless, the two samples show completely different $\rho(T)$ behaviors. *The nonmetallicity of the electron-doped* BiS_2 *layers* in the single crystals is quite puzzling. The ARPES data of our $Eu_3Bi_2S_4F_4$ single crystals show that the intensity of the band dispersion in the energy range of $\sim -0.1 < E < 0$ eV ($= E_F$) is anomalously weakened compared with other BiS_2 systems [40]. This observation may suggest that the doped electrons are localized in this energy range, in reasonable agreement with $E_g = 400$ K [see Fig. 2(b)].

One possible source for the localization is *disorder potentials* in BiS_2 layers induced by randomly distributed Eu^{2+} and Eu^{3+} ions in the nearby block layers. However, the observed $\rho \sim T^{-3}$ is different from $T^{-0.5}$ due to the weak Anderson localization [8,43] or $\exp[(T_0/T)^{1/(d+1)}]$, where T_0 and d are a characteristic energy scale and the spatial dimension ($d = 2$ is expected for the layered material), respectively, due to Mott's variable-range hopping [44]. Another one is *lattice instability*. A band-structure calculation for BiS_2 systems predicts strong electron-phonon coupling and charge-density wave (CDW) instabilities [45]. Actually, one such instability has been confirmed by the observation of the crystalline symmetry lowering from tetragonal to monoclinic in $LaOBiS_2$ [46] and the formation of incommensurate CDW lattice modulations in $LaO_{0.5}F_{0.5}BiS_2$ [47,48] and $NdO_{1-x}F_xBiS_2$ [49]. Although the source of the lattice instabilities has not been clarified yet, some aspects relevant to the source should differ substantially between the single crystals and polycrystals, e.g., the spatial distribution of Eu^{2+}/Eu^{3+} ions, the fluctuation timescale of Eu valence, or the wave vector corresponding to the lattice instability. The unique feature of carriers in the locally noncentrosymmetric BiS_2 layers, i.e., the *spin-texture* caused by the strong spin-orbit coupling [50] might be relevant to the mechanism.

In summary, we have measured electrical resistivity ρ, magnetization M, and specific heat C of $Eu_3Bi_2S_4F_4$ single crystals. The sharp λ-type peak in $C(T)$ appearing at the AFM transition temperature $T_N = 2.17$ K suggests the existence of strong Eu magnetic moment fluctuations due to the quasi-two-dimensional nature of the Eu-ion lattice in Eu_3F_4 block layers. In the AFM state, the anisotropy in M indicates the Eu ordered magnetic moments are aligned along the [001] direction. The average Eu-ion valence $v_{Eu} = +2.19$ has been determined from the magnetic susceptibility $\chi(T)$, saturation magnetization M_{sat}, and the Schottky $4f$-electron contribution to the specific heat. This result suggests the self-doped electron density in BiS_2 layers to be $n = 1.5(v_{Eu} - 2) = 0.285$ electrons per Bi site. Nevertheless, $\rho(T)$ shows an anomalous nonmetallic behavior with T^{-3} dependence below $\sim$100 K without any sign of superconductivity, in marked contrast to a metallic behavior with a superconducting transition at 1.5 K in polycrystals [25]. This finding suggests an unconventional electron-localization mechanism working in the single crystals, possibly caused by Eu^{2+}/Eu^{3+} distribution (or fluctuations) and/or lattice instabilities inherent to BiS_2 layers.

We are grateful to T. Mizokawa and N. L. Saini for fruitful discussions. This work was supported by MEXT JSPS KAKENHI Grants-in-Aid [Grants No. JP15H05884 (J-Physics), No. JP15H03693, No. JP15K05178, No. JP16K05454, No. JP19H01839, No. JP22K03517, and No. JP23H04870] and Tokyo Metropolitan Government Advanced Research (Grant No. H31-1).

[1] Y. Mizuguchi, H. Fujihisa, Y. Gotoh, K. Suzuki, H. Usui, K. Kuroki, S. Demura, Y. Takano, H. Izawa, and O. Miura, BiS_2-based layered superconductor $Bi_4O_4S_3$, Phys. Rev. B **86**, 220510(R) (2012).

[2] Y. Mizuguchi, S. Demura, K. Deguchi, Y. Takano, H. Fujihisa, Y. Gotoh, H. Izawa, and O. Miura, Superconductivity in novel BiS_2-based layered superconductor $LaO_{1-x}F_xBiS_2$, J. Phys. Soc. Jpn. **81**, 114725 (2012).

[3] D. Yazici, I. Jeon, B. D. White, and M. B. Maple, Superconductivity in layered BiS_2-based compounds, Physica C **514**, 218 (2015).

[4] Y. Mizuguchi, Review of superconductivity in BiS_2-based layered materials, J. Phys. Chem. Solids **84**, 34 (2015).

[5] J. G. Bednorz and K. A. Muller, Possible highT_c superconductivity in the Ba-La-Cu-O system, Z. Phys. B **64**, 189 (1986).

[6] Y. Kamihara, T. Watanabe, M. Hirano, and H. Hosono, Iron-based layered superconductor $LaO_{1-x}F_xFeAs$ ($x = 0.05 - 0.12$) with $T_c = 26$ K, J. Am. Chem. Soc. **130**, 3296 (2008).

[7] D. Yazici, K. Huang, B. D. White, I. Jeon, V. W. Burnett, A. J. Friedman, I. K. Lum, M. Nallaiyan, S. Spagna, and M. B. Maple, Superconductivity induced by electron doping in $La_{1-x}M_xOBiS_2$ (M = Ti, Zr, Hf, Th), Phys. Rev. B **87**, 174512 (2013).

[8] H. Sakai, D. Kotajima, K. Saito, H. Wadati, Y. Wakisaka, M. Mizumaki, K. Nitta, Y. Tokura, and S. Ishiwata, Insulator-to-superconductor transition upon electron doping in a BiS_2-based superconductor $Sr_{1-x}La_xFBiS_2$, J. Phys. Soc. Jpn. **83**, 014709 (2014).

[9] H. Usui, K. Suzuki, and K. Kuroki, Minimal electronic models for superconducting BiS_2 layers, Phys. Rev. B **86**, 220501(R) (2012).

[10] T. Sugimoto, D. Ootsuki, C. Morice, E. Artacho, S. S. Saxena, E. F. Schwier, M. Zheng, Y. Kojima, H. Iwasawa, K. Shimada, M. Arita, H. Namatame, M. Taniguchi, M. Takahashi, N. L. Saini, T. Asano, R. Higashinaka, T. D. Matsuda, Y. Aoki, and T. Mizokawa, Fermi surfaces and orbital polarization in superconducting $CeO_{0.5}F_{0.5}BiS_2$ revealed by angle-resolved photoemission spectroscopy, Phys. Rev. B **92**, 041113(R) (2015).

[11] Z. R. Ye, H. F. Yang, D. W. Shen, J. Jiang, X. H. Niu, D. L. Feng, Y. P. Du, X. G. Wan, J. Z. Liu, X. Y. Zhu, H. H. Wen, and M. H. Jiang, Electronic structure of single-crystalline $NdO_{0.5}F_{0.5}BiS_2$ studied by angle-resolved photoemission spectroscopy, Phys. Rev. B **90**, 045116 (2014).

[12] M. Nagao, A. Miura, S. Demura, K. Deguchi, S. Watauchi, T. Takei, Y. Takano, N. Kumada, and I. Tanaka, Growth and superconducting properties of F-substituted $ROBiS_2$ (R = La, Ce, Nd) single crystals, Solid State Commun. **178**, 33 (2014).

[13] M. Nagao, M. Tanaka, S. Watauchi, I. Tanaka, and Y. Takano, Superconducting anisotropies of F-substituted $LaOBiSe_2$ single crystals, J. Phys. Soc. Jpn. **83**, 114709 (2014).

[14] R. Higashinaka, T. Asano, T. Nakashima, K. Fushiya, Y. Mizuguchi, O. Miura, T. D. Matsuda, and Y. Aoki, Pronounced -Log$T$ divergence in specific heat of nonmetallic $CeOBiS_2$: A mother phase of BiS_2-based superconductor, J. Phys. Soc. Jpn. **84**, 023702 (2015).

[15] T. Sugimoto, D. Ootsuki, E. Paris, A. Iadecola, M. Salome, E. F. Schwier, H. Iwasawa, K. Shimada, T. Asano, R. Higashinaka, T. D. Matsuda, Y. Aoki, N. L. Saini, and T. Mizokawa, Localized and mixed valence state of Ce $4f$ in superconducting and ferromagnetic $CeO_{1-x}F_xBiS_2$ revealed by x-ray absorption and photoemission spectroscopy, Phys. Rev. B **94**, 081106(R) (2016).

[16] T. Sugimoto, E. Paris, T. Wakita, K. Terashima, T. Yokoya, A. Barinov, J. Kajitani, R. Higashinaka, T. D. Matsuda, Y. Aoki, T. Mizokawa, and N. L. Saini, Metallic phase in stoichiometric $CeOBiS_2$ revealed by space-resolved ARPES, Sci. Rep. **8**, 2011 (2018).

[17] A. Miura, M. Nagao, Y. Goto, Y. Mizuguchi, T. D. Matsuda, Y. Aoki, C. Moriyoshi, Y. Kuroiwa, Y. Takano, S. Watauchi, I. Tanaka, N. C. Rosero-Navarro, and K. Tadanaga, Crystal structure and superconductivity of tetragonal and monoclinic $Ce_{1-x}Pr_xOBiS_2$, Inorg. Chem. **57**, 5364 (2018).

[18] H. F. Zhai, Z. T. Tang, H. Jiang, K. Xu, K. Zhang, P. Zhang, J. K. Bao, Y. L. Sun, W. H. Jiao, I. Nowik, I. Felner, Y. K. Li, X. F. Xu, Q. Tao, C. M. Feng, Z. A. Xu, and G. H. Cao, Possible charge-density wave, superconductivity, and f-electron valence instability in $EuBiS_2F$, Phys. Rev. B **90**, 064518 (2014).

[19] H. F. Zhai, P. Zhang, and G. H. Cao, Superconductivity in europium bismuth sulfofluorides, J. Phys. Soc. Jpn. **88**, 041003 (2019).

[20] T. Sugimoto, E. Paris, K. Terashima, A. Barinov, A. Giampietri, T. Wakita, T. Yokoya, J. Kajitani, R. Higashinaka, T. D. Matsuda, Y. Aoki, T. Mizokawa, and N. L. Saini, Inhomogeneous charge distribution in a self-doped $EuFBiS_2$ superconductor, Phys. Rev. B **100**, 064520 (2019).

[21] S. Demura, Ordered states coexisting with superconductivity in $BiCh_2$ materials, J. Phys. Soc. Jpn. **88**, 041002 (2019).

[22] J. Xing, S. Li, X. Ding, H. Yang, and H.-H. Wen, Superconductivity appears in the vicinity of semiconducting-like behavior in $CeO_{1-x}F_xBiS_2$, Phys. Rev. B **86**, 214518 (2012).

[23] S. Demura, K. Deguchi, Y. Mizuguchi, K. Sato, R. Honjyo, A. Yamashita, T. Yamaki, H. Hara, T. Watanabe, S. J. Denholme, M. Fujioka, H. Okazaki, T. Ozaki, O. Miura, T. Yamaguchi, H. Takeya, and Y. Takano, Coexistence of bulk superconductivity and magnetism in $CeO_{1-x}F_xBiS_2$, J. Phys. Soc. Jpn. **84**, 024709 (2015).

[24] R. Jha and V. P. S. Awana, Superconductivity in layered $CeO_{0.5}F_{0.5}BiS_2$, J. Supercond. Novel Magn. **27**, 1 (2014).

[25] H. F. Zhai, P. Zhang, S. Q. Wu, C. Y. He, Z. Tu. Tang, H. Jiang, Y. L. Sun, J. K. Bao, I. Nowik, I. Felner, Y. W. Zeng, Y. K. Li, X. F. Xu, Q. Tao, Z. A. Xu, and G. H. Cao, Anomalous Eu valence state and superconductivity in undoped $Eu_3Bi_2S_4F_4$, J. Am. Chem. Soc. **136**, 15386 (2014).

[26] K. Ishigaki, J. Gouchi, K. Torizuka, S. Arumugam, A. K. Ganguli, G. Kalaiselvan, Z. Haque, G. S. Thakur, L. C. Gupta, and Y. Uwatoko, Pressure effect on the BiS_2 layered compound $Eu_3Bi_2S_4F_4$, JPS Conf. Proc. **30**, 011058 (2020).

[27] Y. Luo, H. F. Zhai, P. Zhang, Z. A. Xu, G. H. Cao, and J. D. Thompson, Pressure-enhanced superconductivity in $Eu_3Bi_2S_4F_4$, Phys. Rev. B **90**, 220510(R) (2014).

[28] P. Zhang, H. F. Zhai, Z. J. Tang, L. Li, Y. K. Li, Q. Chen, J. Chen, Z. Wang, C. M. Feng, G. H. Cao, and Z. A. Xu, Superconductivity enhanced by Se doping in $Eu_3Bi_2(S, Se)_4F_4$, Europhys. Lett. **111**, 27002 (2015).

[29] Z. Haque, G. S. Thakur, R. Parthasarathy, B. Gerke, T. Block, L. Heletta, R. Pöttgen, A. G. Joshi, G. K. Selvan, S. Arumugam, L. C. Gupta, and A. K. Ganguli, Unusual mixed valence of Eu in two materials–$EuSr_2Bi_2S_4F_4$ and $Eu_2SrBi_2S_4F_4$: Mössbauer and x-ray photoemission spectroscopy investigations, Inorg. Chem. **56**, 3182 (2017).

[30] Z. Haque, G. S. Thakur, G. K. Selvan, T. Block, O. Janka, R. Pöttgen, A. G. Joshi, R. Parthasarathy, S. Arumugam, L. C. Gupta, and A. K. Ganguli, Valence state of Eu and superconductivity in se-substituted $EuSr_2Bi_2S_4F_4$ and $Eu_2SrBi_2S_4F_4$, Inorg. Chem. **57**, 37 (2018).

[31] P. Zhang, H. F. Zhai, Z. Wang, J. Chen, C. M. Feng, G. H. Cao, and Z. A. Xu, Effect of Sr doping in layered $Eu_3Bi_2S_4F_4$ superconductor, Supercond. Sci. Technol. **30**, 015005 (2017).

[32] M. Nagao, Growth and characterization of R(O, F)BiS_2 (R = La, Ce, Pr, Nd) superconducting single crystals, Nov. Supercond. Mater. **1**, 64 (2015).

[33] M. Nagao, M. Tanaka, S. Watauchi, Y. Takano, and I. Tanaka, Growth and superconducting properties of Cd-doped La(O, F)BiS_2 single crystals, Solid State Commun. **261**, 32 (2017).

[34] Y. C. Chan, K. Y. Yip, Y. W. Cheung, Y. T. Chan, Q. Niu, J. Kajitani, R. Higashinaka, T. D. Matsuda, Y. Yanase, Y. Aoki, K. T. Lai, and S. K. Goh, Anisotropic two-gap superconductivity and the absence of a Pauli paramagnetic limit in single-crystalline $LaO_{0.5}F_{0.5}BiS_2$, Phys. Rev. B **97**, 104509 (2018).

[35] F. Giubileo, F. Romeo, A. Di Bartolomeo, Y. Mizuguchi, and P. Romano, Probing unconventional pairing in $LaO_{0.5}F_{0.5}BiS_2$ layered superconductor by point contact spectroscopy, J. Phys. Chem. Solids **118**, 192 (2018).

[36] R. Higashinaka, H. Endo, J. Kajitani, T. D. Matsuda, and Y. Aoki, Single crystal growth and physical properties of BiS_2-layered compound $Eu_3Bi_2S_4F_4$, Phys. B: Condens. Matter **536**, 824 (2018).

[37] See Supplemental Material at http://link.aps.org/supplemental/10.1103/PhysRevB.108.L081122 for the characterization of single crystals, the Van Vleck paramagnetic susceptibility for a free Eu^{3+} ion,the specific heat data analyses, and a concave upward curvature of the [001] magnetization curves. It also contains Refs. [38,39].

[38] J. H. Van Vleck, in *The Theory of Electric and Magnetic Susceptibilities* (Oxford University Press, Oxford, 1932), p. 226.

[39] B. Bleaney, Hyperfine Interactions in rare-earth metals, J. Appl. Phys. **34**, 1024 (1963).

[40] E. Paris, T. Sugimoto, T. Wakita, A. Barinov, K. Terashima, V. Kandyba, O. Proux, J. Kajitani, R. Higashinaka, T. D. Matsuda, Y. Aoki, T. Yokoya, T. Mizokawa, and N. L. Saini, Electronic structure of self-doped layered $Eu_3F_4Bi_2S_4$ material revealed by x-ray absorption spectroscopy and photoelectron spectromicroscopy, Phys. Rev. B **95**, 035152 (2017).

[41] Y. Takikawa, S. Ebisu, and S. Nagata, Van Vleck paramagnetism of the trivalent Eu ions, J. Phys. Chem. Solids **71**, 1592 (2010).

[42] Y. Aoki, H. R. Sato, H. Sugawara, and H. Sato, Anomalous magnetic properties of Heusler superconductor $YbPd_2Sn$, Physica C: Superconduct. **333**, 187 (2000).

[43] P. A. Lee and T. V. Ramakrishnan, Disordered electronic systems, Rev. Mod. Phys. **57**, 287 (1985).

[44] N. F. Mott, *Metal-Insulator Transitions* (Taylor & Francis, London, 1974).

[45] T. Yildirim, Ferroelectric soft phonons, charge density wave instability, and strong electron-phonon coupling in BiS_2 layered superconductors: A first-principles study, Phys. Rev. B **87**, 020506(R) (2013).

[46] R. Sagayama, H. Sagayama, R. Kumai, Y. Murakami, T. Asano, J. Kajitani, R. Higashinaka, T. D. Matsuda, and Y. Aoki, Symmetry lowering in $LaOBiS_2$: A mother material for BiS_2-based layered superconductors, J. Phys. Soc. Jpn. **84**, 123703 (2015).

[47] J. Kajitani, R. Sagayama, H. Sagayama, K. Matsuura, T. Hasegawa, R. Kumai, Y. Murakami, M. Mita, T. Asano, R. Higashinaka, T. D. Matsuda, and Y. Aoki, Transverse-type lattice modulation in $LaO_{0.5}F_{0.5}BiS_2$: Possible charge density wave formation, J. Phys. Soc. Jpn. **90**, 103601 (2021).

[48] H. Tamatsukuri, T. Hasegawa, H. Sagayama, M. Mizumaki, Y. Murakami, J. Kajitani, R. Higashinaka, T. D. Matsuda, Y. Aoki, and S. Tsutsui, Investigation of the phonon dispersion associated with superlattice reflections in the BiS_2-based superconductor $LaBiS_2O_{0.5}F_{0.5}$, Phys. Rev. B **107**, 024303 (2023).

[49] J. Lee, M. Nagao, Y. Mizuguchi, and J. Ruff, Direct observation of an incommensurate charge density wave in the BiS_2-based superconductor $NdO_{1-x}F_xBiS_2$, Phys. Rev. B **103**, 245120 (2021).

[50] X. Zhang, Q. Liu, J.-W. Luo, A. J. Freeman, and A. Zunger, Hidden spin polarization in inversion-symmetric bulk crystals, Nat. Phys. **10**, 387 (2014).